



UNIVERSITY OF LEEDS

This is a repository copy of *Deformation of 3D printed agglomerates: Multiscale experimental tests and DEM simulation*.

White Rose Research Online URL for this paper:  
<http://eprints.whiterose.ac.uk/157178/>

Version: Accepted Version

---

**Article:**

Ge, R, Ghadiri, M [orcid.org/0000-0003-0479-2845](https://orcid.org/0000-0003-0479-2845), Bonakdar, T et al. (4 more authors) (2020) Deformation of 3D printed agglomerates: Multiscale experimental tests and DEM simulation. *Chemical Engineering Science*, 217. 115526. ISSN 0009-2509

<https://doi.org/10.1016/j.ces.2020.115526>

---

© 2020 Elsevier Ltd. All rights reserved. This manuscript version is made available under the CC-BY-NC-ND 4.0 license <http://creativecommons.org/licenses/by-nc-nd/4.0/>.

**Reuse**

This article is distributed under the terms of the Creative Commons Attribution-NonCommercial-NoDerivs (CC BY-NC-ND) licence. This licence only allows you to download this work and share it with others as long as you credit the authors, but you can't change the article in any way or use it commercially. More information and the full terms of the licence here: <https://creativecommons.org/licenses/>

**Takedown**

If you consider content in White Rose Research Online to be in breach of UK law, please notify us by emailing [eprints@whiterose.ac.uk](mailto:eprints@whiterose.ac.uk) including the URL of the record and the reason for the withdrawal request.



[eprints@whiterose.ac.uk](mailto:eprints@whiterose.ac.uk)  
<https://eprints.whiterose.ac.uk/>

# **Deformation of 3D Printed Agglomerates: Multiscale Experimental Tests and DEM Simulation**

Ruihuan Ge<sup>1</sup>, Mojtaba Ghadiri<sup>2</sup>, Tina Bonakdar<sup>2</sup>, Qijun Zheng<sup>3</sup>, Zongyan Zhou<sup>3</sup>,  
Ian Larson<sup>4</sup> & Karen Hapgood<sup>1,5\*</sup>

1 Department of Chemical Engineering, Monash University, Australia

2 School of Chemical and Process Engineering, University of Leeds, UK

3 Laboratory for Simulation and Modelling of Particulate Systems, Department of Chemical Engineering, Monash University, Australia

4 Drug Delivery, Disposition and Dynamics, Monash Institute of Pharmaceutical Sciences, Monash University, Australia

5 School of Engineering, Deakin University, Australia

E-mail: karen.hapgood@deakin.edu.au

## **ABSTRACT**

Agglomerates are widely used in industry, and their mechanical properties are of great interest. In this work, we propose a new concept of using a coordinated multiscale approach to match the physical and digital agglomerate structures and properties. By using a multi-material 3D printing technology, the inter-particle bond properties and agglomerate structures could be precisely controlled and replicated. Quasi-static compression tests have been carried out for the 3D printed samples at different scales. A Timoshenko Beam Bond Model (TBBM) with bond properties matching those of the 3D printed agglomerates is used for describing bond deformation. Discrete Element Method (DEM) is then employed to simulate the agglomerate crushing process. The results show that for both agglomerate structures, the DEM simulation and experimental results show good agreement at the initial elastic deformation stage. This work opens up the chance for significant advances in agglomerate deformation and breakage modelling in future.

## **KEYWORDS**

3D printing; Discrete Element Method (DEM); Agglomerates; Deformation

## 1. INTRODUCTION

Agglomeration is a common process in chemical and allied industries, in which small particles are combined together into larger entities called “granules” or “agglomerates”. During the processing of these granules, their mechanical properties including deformation and breakage play an important role in handling and transportation (Reynolds et al., 2005). Agglomerates have complex structures and bond mechanics. While past experimental and modelling efforts attempted to analyse agglomerate strength, reliable methods to precisely predict agglomerate deformation or breakage have yet to be developed. Particularly, the approach of Discrete Element Method (DEM) originally proposed by (Cundall and Strack, 1979) has been widely used to investigate agglomeration and breakage behaviour due to its unique advantage in generating detailed particle scale information including deformation and force structure.

DEM models the motion, collisions and the resulting contact forces between particles, for which a contact model is required. Several contact models have been developed and applied for describing cohesive forces between fine powders, e.g. Johnson-Kendall-Roberts (JKR) model considering strong short-range adhesive forces within the contact area, Derjaguin-Muller-Toporov (DMT) model including long-range surface forces (Derjaguin et al., 1975; Johnson et al., 1971; Matuttis and Schinner, 2001). JKR model (Johnson et al., 1971) is one of the most commonly used cohesive models for simulating the agglomerate breakage. Using this model, the effects of several influential factors including impact conditions, structure, shape and surface energy have been analysed (Liu et al., 2010; Mishra and Thornton, 2001; Thornton et al., 2004; Thornton and Liu, 2004; Thornton et al., 1996). Furthermore, the relationship between the inter-particle surface energy and impact breakage of an agglomerate was quantitatively described by the Weber Number (Kafui and Thornton, 1993). Modified Weber numbers were proposed by Moreno-Atanasio & Ghadiri (Moreno-Atanasio and Ghadiri, 2006) and Subero *et al.* (Subero et al., 1999) to give a better unification of model predictions over a range of different agglomerates and impact conditions.

Although extensive DEM studies have been conducted, the main limitation of previous research is that most JKR model based simulations are difficult to be validated via experiments. Ning et al. (Ning et al., 1997) compared the simulation and experimental results of weak lactose agglomerates without binders. The macroscopic impact breakage patterns and extents of breakage showed a good agreement between simulation and experiment. Golchert *et al.*

(Golchert et al., 2004) were the first to investigate the breakage of agglomerates with binders by characterising the agglomerate structure using X-ray micro-tomography. The 3D spatial locations of particles of the actual agglomerate were implemented into the DEM code, which provided the exact geometries for simulating the agglomerate failure behaviour under compression. The results were then used to compare with those obtained from experiments. Despite having identical structures, the results showed vastly different behaviours for the real and the simulated agglomerate. During the simulation, cohesive contacts are continually made and broken. This implies that the JKR model is not suitable for describing the breakage of agglomerates with solid binder bridges, where the primary particles are not in direct contact but held apart by a solid bridge, which can undergo irreversible breakage if the deformation is large enough.

Bond models are more suitable for modelling agglomerates with physical bridges between the particles. Compared to cohesive models, bond models consist of a rigid bond between primary particles that is only formed once (usually at the start of a simulation) and persists until breakage happens. A series of bond models have been developed, e.g. simple spring model (Ergenzinger et al., 2011), parallel bond model represented by a pair of springs (Potyondy and Cundall, 2004) and beam model by the use of Euler-Bernoulli or Timoshenko beam elements (Brown et al., 2014). The most widely used bond model in agglomerate breakage research is the Linear Parallel Bond (LPB) model proposed by Potyondy and Cundall (Potyondy and Cundall, 2004). In this model, particles are connected by a set of elastic springs with constant shear and normal stiffness. Dosta *et al.* (Dosta et al., 2016) applied the LPB to predict the agglomerate strength with realistic microstructures and inter-particle bonds using DEM simulation of agglomerate compression. The particle position, binder and porosity distributions within the agglomerates were obtained by the X-ray micro-tomography (Dale et al., 2014). While simulations and experiments lacked close quantitative agreement, both showed a similar qualitative increase in strength with increasing binder contents. Calibration methods to obtain the bonding parameters of LPB model do not take account of the inherent physical properties of contacts and hence the ability to predict the correct outcome was limited (Dosta et al., 2016; Eckhard et al., 2017). The beam model provides a more realistic representation of bond mechanics. Recently Brown *et al.* (Brown et al., 2014) developed a Timoshenko Beam Bond Model (TBBM) based on Timoshenko beam theory. The TBBM is suitable to describe the deformation of stubby beams. It can transmit normal, shear, bending and torsion forces to neighbouring particles (Przemieniecki, 1985). Three strength criteria are considered in this

model including compressive, shear and tensile strength. By comparison, the LPB model can only transit normal and shear stiffness, and resist tensile and shear strength of the bonds. The TBBM is used in our research, due to the physical similarity between the beam model and the inter-particle bonds we have designed in our agglomerates.

In order to validate DEM simulation results, it is necessary to experimentally have a precise control of the agglomerate structure and inter-particle bond properties. This enables a systematic investigation of the influence of each parameter including structure and bond properties on the agglomerate mechanical properties, and helps to improve simulations of agglomerate breakage and bond deformation models. Subero *et al.* (Subero et al., 2000) investigated the effect of structure on the impact strength of agglomerates using model agglomerates made of glass ballotini glued together by an epoxy resin binder. Although the results were promising, the agglomerates were made using a moulding technique, and the complex internal structure and inter particle bond properties could not be controlled and reproduced. Recently, we proposed 3D printing technology as a way to produce complex structures with tuneable mechanical properties (Ge et al., 2017). A multi-material 3D printing technology was used to print customised agglomerates with a number of rigid primary particles connected by rubber-like inter-particle bonds. The agglomerate strength can be systematically “tuned” by varying structure and/or material properties independently. For instance, the inter-particle bond properties can be varied while keeping the agglomerate structure identical. In this work, we used the ideal cylindrical bond which is a simplification of the complex agglomerate system. In reality, the inter-particle solid bonds have complex geometries (e.g. full or hollow, single or clustered) (Dadkhah and Tsotsas, 2014; Farber et al., 2003) depending on the process parameters. As the 3D printing method provides a rigorous way for controlling the physical properties of agglomerates, more complex bond geometries can be considered in future. Despite some anisotropy from the 3D printing layer direction, the original report (Ge et al., 2017) showed that this 3D printing method produces novel, highly reproducible agglomerates which can be used to facilitate far more rigorous testing and comparison of agglomerate breakage models. The new method allows researchers to conduct simulations on a “digital twin” of a physical agglomerate, and to manipulate the physical properties as easily as the digital properties-something that has not been done before.

In this study, we expand this experimental approach by characterising the 3D printed samples at three different scales, and specifically compare the deformation response of 3D printed

agglomerates with DEM simulation predictions. The 3D printing material properties were carefully measured at the single material scale, and the Young's modulus values were obtained. The properties of a single bond between two particles, called a "doublet" were measured and Finite Element Method (FEM) of the doublet compression was used to determine the linear-elastic limit. The bonding parameters in the linear elastic range were then used in the TBBM model and fed into DEM simulations of the agglomerate deformation. Two different agglomerate types, one a cubic shape with an internal tetrahedral structure and another a spherical shape with a randomly packed structure were designed and 3D printed, and subjected to quasi-static compression tests. DEM simulations of the agglomerate crushing were carried out under identical strain conditions and the predictions were compared with the corresponding experimental results. The results demonstrate that this multiscale experimental approach is a promising way to verify and advance DEM simulations of the elastic deformation of agglomerate structures.

## **2. METHODOLOGY**

### **2.1 3D printing and agglomerate production**

A PolyJet multi-material 3D printing technology (Stratasys Objet 500) was used to print the agglomerates. This is one of the most advanced printers currently on the market, with a printing resolution of 600 dpi in the X and Y directions and 1600 dpi in Z direction (30  $\mu\text{m}$  layer thickness). This PolyJet 3D printer can print up to 14 different polymer materials with varied mechanical properties simultaneously. Visually, the bonds inside agglomerates are smooth and cylindrical. The samples are far more reproducible than any experimental system produced to date. To further evaluate the accuracy, cylindrical geometries of different dimensions were printed and measured by a digital calliper with a 10  $\mu\text{m}$  measurement accuracy. As shown in Table 1, the hatched lines within the geometry indicate the 3D printing layer planes with respect to the loading direction. The horizontal and vertical alignments refer to the two cases where the layers have been printed with perpendicular or parallel to the cylinder axis, along which the load is applied. For all cases the "horizontal alignment" samples are mainly used in the following sections as they have a higher accuracy. Although there are some deviations found for the "vertical alignment" samples, the model size accuracy is within 100  $\mu\text{m}$ . The deviations may affect the results slightly, but the control of the test sample dimensions is unprecedented and the variation in this study is less than any equivalent experimental system produced to date.

<Table 1. Measurement dimensions of 3D printed cylinders.>

In this research, the primary particles (particle diameter  $d_p=4$  mm) were printed using a rigid polymer VeroWhitePlus™ while a rubber-like DM 9895 was used to print the cylindrical bonds (bond diameter  $d_b=2.6$  mm) between the primary particles. Material properties of these two materials are listed in Tables 2 and 3. Details of the agglomerate designs, printing and cleaning methods have been reported previously (Ge et al., 2017). As shown in Figure 1, two different agglomerate structures were designed and used, i.e. a cube-shaped agglomerate with a tetrahedral internal structure and a spherical agglomerate with a random internal structure.

The cubic tetrahedral structured agglomerate (Figure 1 (a)) was designed within SolidWorks using 91 spherical primary particles, each 4 mm in diameter. The particles were connected by cylindrical inter-particle bonds with a diameter ( $d_b$ ) of 2.6 mm. The bond length ( $l$ ) corresponding to the minimum distance between neighbouring particle surfaces was 0.25 mm. Note that bond length  $l$  refers to the experimental case, which is different for the adjacent primary particles center-to-center bond length ( $L_b$ ) used in DEM simulations.  $L_b$  can be calculated as the sum of the bond length  $l$  plus the radii of the two particles attached to the bond.

The spherical agglomerate (Figure 1 (b)) was made of 120 spherical primary particles, also all 4 mm in diameter, having a random structure with an average bond length of  $l=0.25$  mm. The agglomerate was generated using the “dynamic particle factory” function in EDEM software package (DEM Solutions, Edinburgh, UK), where the particles were densely assembled within a 25 mm spherical space. During the generation process, a gravity field was assigned and changed in different directions to ensure the particles filled the whole space. After generating the dense structure, a surface energy according to the JKR contact model was assigned to these particles. The spherical geometry and gravity field were then removed, and the surface energy was set to zero. After that, particles repelled each other mutually and moved away from each other until the average bond length  $l$  increased to 0.25 mm. The generated particle positions were then exported to Solidworks. Particles within 4.6 mm of each other (centre to centre distance) were considered to be joined by a 2.6 mm diameter bond. As the spherical agglomerate has a random structure, it is hardly to control all bonds have the same length. In this work, the generated structure has a narrow distribution of bond length with an average

value of  $l=0.25$  mm. Once the final agglomerate design was completed, the print materials for the primary particles and bonds were specified and the final design was imported as an STL file, ready for 3D printing. At least three identical copies of each agglomerate type were printed in order to perform replicate breakage tests. A general design overview and production process of the spherical agglomerates with random structure are illustrated in Figure 2.

<Figure 1. Agglomerate design used in this study: (a) cubic agglomerate with tetrahedral internal structure, and (b) spherical agglomerate with random internal structure.>

<Figure 2. Overview of the design and production process for spherical agglomerates with random internal structure.>

## **2.2 Mechanical testing at three different scales**

Using 3D printing, complex agglomerate structures and their sub-models can be isolated and fabricated according to the test requirements. The 3D printed test samples of three different scales are illustrated in Figure 3. Mechanical tests were performed on these 3D printed samples using an Instron 5566 universal tester. In this work, the tests were carried out quasi-statically at a fixed loading rate of 0.02 mm/s. The effect of strain rate on agglomerate properties has been presented elsewhere (Ge et al., 2018). Three different load cells (i.e. 100 N, 1000 N and 10000 N) were used according to the load cell selection criteria for appropriate resolution (Instron Corporation, 2005). The 3D printer builds the objects by applying successive layers of each polymer on top of each other to create the final geometry. The printed layer directions relative to the applied loading direction may affect the experimental results. The effect of print layer orientation relative to the compression direction was investigated by (Ge et al., 2017). Here, most samples were tested under the orientation in which the printed layers aligned horizontally with the platen, i.e. the loading direction was perpendicular to the print layers. To evaluate the 3D printing layer effect, some tests with printed layers parallel to the loading directions were also conducted. In the following, “perpendicular loading” means that the applied load is perpendicular to the printed layers, while “parallel loading” means that the loading direction and printed layers planes are parallel. A schematic of these two loading directions is shown in Figure 4.



<Figure 3. 3D printed test samples at three different scales. White material is a rigid polymer (Vero WhitePlus™), and black material is a rubber-like polymer (DM 9895).>

<Figure 4. Schematic of loading direction with respect to 3D printed layers inside a cylindrical geometry.>

As illustrated in Figure 3 (a), samples of single materials of the 3D printing polymers with different geometries were printed and characterised under uniaxial compression and tensile test conditions to obtain their Young's modulus values. Two small cylinders (10 mm high, 10 mm diameter) were printed, one using the rigid VeroWhite polymer (used for printing the primary particles) and the other using the rubber-like DM 9895 polymer (used for printing the bonds), both tested under uniaxial compression conditions. In addition, “dog bone” shaped specimens of the bond material were printed and tested under tensile conditions according to ASTM D638 (ASTM, 2008) standard.

As depicted in Figure 3 (b), doublets (two particles bound by a single bond) with the same bond diameter but different bond lengths were printed and tested to obtain the bond deformation and failure characteristics. The samples were fabricated in two different shapes to suit compression/tensile testing. For all the tested samples, the primary particle material was rigid VeroWhite polymer, and the bond material was rubber-like DM 9895. The bond diameter  $d_b$  was 2.6 mm (matching bond diameter in the agglomerate), and four different bond lengths ( $l=0, 0.25, 0.5, 1$  mm) were considered (See Figure 3 (b)). Here, the bond length,  $l$ , represents the minimum distance between the outer surfaces of the two adjacent particles.

Quasi-static compression tests were performed on the 3D printed agglomerates (see Figure 3 (c)) to obtain the load displacement curves. As shown in Figure 5, the upper plate was moved at a loading rate of 0.02 mm/s, and agglomerates were individually compressed between two rigid plates. The compressive load of the top plate was recorded and analysed. In order to have consistent conditions, all the agglomerates were tested with the printed layers perpendicular to the loading direction (see Figure 5). For each experiment, at least three replicates (using identical printed copies of each agglomerate design) were performed to ensure repeatability.

<Figure 5. Schematic of test setup, showing the horizontal alignment of the print layers with the testing platens.>

## 2.3 Discrete Element Method (DEM) simulation

### 2.3.1 The TBBM contact model

DEM simulations were carried out using EDEM software and the TBBM model to describe the bond deformation between primary particles. In the TBBM, a Timoshenko beam element is used to connect the centres of two primary particles. In this way, the bond ends share the same degrees of freedom with corresponding particles (Brown et al., 2014) .

A schematic diagram of a bond beam is shown in Figure 6. The bond length in the TBBM model,  $L_b$ , is defined as the distance between two primary particle centres. The contact radius is used as a criterion to bond the particles. As shown in Figure 6, the contact radius have a value that is slightly greater than the physical radius of particles. Particles can be bonded together when their contact radii overlap. To ensure the agglomerate structures in simulation have the same number of bonds as the corresponding 3D printed agglomerates, the contact radius of the agglomerate structure in DEM simulation was set to 2.15 mm for the cubic tetrahedral agglomerate, to match the experimental arrangement of a 0.25 mm length bond between two 4 mm diameter particles. Similarly, the contact radius was set to 2.28 mm for the spherical random structured agglomerates to ensure a 0.25 mm average bond length.

<Figure 6. Schematic of a single beam connecting particles together. Particles are bonded together when the contact radius overlaps. The solid circle shows the actual particles, while the broken circle radius and overlap are used to define the bond length. (Particle diameter  $2*r_p= 4$  mm, bond radius  $r_b=1.3$  mm, contact radius is 2.15 mm and 2.28 mm for cubic tetrahedral structure and spherical random structure, respectively)>

At each time step of the simulation, the relationship between the bond displacement  $\Delta u$  and resulting force  $\Delta F$  is described as:

$$\{\Delta F\} = [K] \cdot \{\Delta u\} \quad (1)$$

where  $\{\Delta F\}$  is the incremental force vector that contains six force components ( $\Delta F_i$ ) and six moment ( $\Delta M_i$ ) increments at the two bond ends:

$$\{\Delta F\} = \left\{ \Delta F_{\alpha x}, \Delta F_{\alpha y}, \Delta F_{\alpha z}, \Delta M_{\alpha x}, \Delta M_{\alpha y}, \Delta M_{\alpha z}, \Delta F_{\beta x}, \Delta F_{\beta y}, \Delta F_{\beta z}, \Delta M_{\beta x}, \Delta M_{\beta y}, \Delta M_{\beta z} \right\}^T \quad (2)$$

where  $\alpha$  or  $\beta$  means the two bond ends, and  $x, y$  or  $z$  means the force direction in the coordinate system.  $\{\Delta u\}$  is the incremental displacement vector that contains six displacements and six rotation increments at the two bond ends in the Cartesian space. The stiffness matrix  $[K]$  is a  $12 \times 12$  matrix that can be expressed as a function of the axial, shear and bending forces of the beam. A detailed definition of the stiffness constants and their corresponding forces and moments inside this matrix is given by Przemieniecki (Przemieniecki, 1985).

Three stress components are considered in the TBBM, specifically the compressive ( $\sigma_C$ ), tensile ( $\sigma_T$ ) and shear stress ( $\tau$ ). Detailed equations of the bond stress are given as follows (Brown et al., 2014):

$$\sigma_{Ci} = \left( \frac{F_{\beta x}}{A_b} - \frac{r_b \sqrt{M_{iy}^2 + M_{iz}^2}}{I_b} \right) i = \alpha, \beta \quad (3)$$

$$\sigma_{Ti} = \left( \frac{F_{\beta x}}{A_b} + \frac{r_b \sqrt{M_{iy}^2 + M_{iz}^2}}{I_b} \right) i = \alpha, \beta \quad (4)$$

$$\sigma_{Cmax} = -\min(\sigma_{C\alpha}, \sigma_{C\beta}) \quad (5)$$

$$\sigma_{Tmax} = \max(\sigma_{T\alpha}, \sigma_{T\beta}) \quad (6)$$

$$\tau_{max} = \frac{|M_{\alpha x}| r_b}{2I_b} + \frac{4\sqrt{F_{\alpha y}^2 + F_{\alpha z}^2}}{3A_b} \quad (7)$$

In these equations, the total forces  $F_i$  and moments  $M_i$  are the sum of the incremental forces  $\{\Delta F\}$  at each time step. Equation (5-7) is used to determine the maximum bond stress. In Equation (7), the maximum shear stress  $\tau_{\max}$  is a combination of torsional stress and direct shear stress. The bond between particles fails once the maximum bond stress exceeds the given strength. This work focuses on the deformation of agglomerates without bond failures. The comparison of agglomerate breakage between experiments and DEM simulations is presented in another piece of work (Ge et al., 2019).

### 2.3.2 DEM simulation parameters

Simulations were carried out using EDEM 2.7. The input parameters for the DEM simulation, including those for the inter-particle bonds in the TBBM model, are listed in Table 2. In this table, the bond radius multiplier is defined as the ratio of the bond radius to the primary particle radius. The bonding parameters are based on experimental measurements and the material datasheets given by the 3D printing vendor (Takezawa et al., 2015; Wang et al., 2011). Mechanical properties of steel plates were taken from the material library of EDEM software, and mechanical properties of the primary particles including Young's modulus and Poisson's ratio were supplied by the 3D printing vendor (see Table 2). The sensitivities of parameters including static friction and coefficient of restitution were examined, and it was found these parameters were insensitive within the examined range (i.e. static friction range 0.1-0.5, and restitution coefficient range 0.1-0.9). The time step was calculated based on the criteria offered by (Brown, 2013). Here, a very conservative time step  $1 \times 10^{-7}$  s with a time step multiplier less than 0.01 was chosen. To save computational resource, a 2 mm/s loading rate was used. The DEM simulations subjected the agglomerates to a quasi-static compression. A sensitivity test simulation shown that the results are not dependent on the loading rate within the range of 0.02-2 mm/s loading rate. This is shown in Figure 7, where the resultant force on the rigid platen at the top of the agglomerate is recorded and plotted as a function of the platen displacement.

<Table 2. Parameters used in DEM simulation>

<Figure 7. Comparison of simulated load-displacement curves as a function of loading rate for cubic shaped, tetrahedral structured agglomerate.>

## **2.4 Finite Element Method (FEM) simulation**

The TBBM model used in the DEM simulations assumes linear elastic behaviour. Preliminary results of agglomerate compression to failure showed a highly non-linear response, where the TBBM model is not valid. FEM analysis was used to define the limit of linear-elastic deformation of the 3D printed bonds, and thus the deformation range over which the TBBM was valid. The simulations were performed by using the dynamic explicit method of Abaqus package (Dassault Systemes, USA). The doublet geometry and test conditions were kept the same as experimental tests.

A typical FEM simulation model is illustrated in Figure 8. This model has a flat bottom, which is in accordance with the doublet sample used in compression experiments (see Figure 3 (b)). An axisymmetric finite element model was used due to the cylindrical symmetry of doublets. This geometry was meshed using quadrilateral elements of CAX4R. Mesh sensitivity analysis was carried out and found that the FEM results could converge when the mesh element number was larger than 400. Here, to ensure the reliability, a sufficiently fine mesh (>2000 mesh elements) was used. The linear elastic response of doublets under tensile and compression conditions was then obtained and compared with experimental results. The material Young's modulus values used in FEM and detailed comparisons are given in the following results and analysis section.

<Figure 8. An axisymmetric FEM mesh setup used in doublet compression simulations.>

## **3. RESULTS AND ANALYSIS**

### **3.1 3D printing materials characterisation**

Experimental compressive stress-strain curves of cylindrical geometries (10 mm high, 10 mm diameter) are shown in Figure 9. The engineering stress and strain values are used in this work. During the tests, the printed layers were kept perpendicular to the loading direction. For the rigid polymer used to print the spherical particles, it shows elastic behaviour at the beginning, and then yielding behaviour (see Figure 9 (a)). The value of Young's modulus in the linear

region is around 1 GPa. This value is used in the following FEM and DEM simulations. For the rubber-like polymer used to print the inter-particle bonds, the measured stress-strain curve is shown in Figure 9 (b). A line is fitted to the initial Hookean region up to 0.2 strain, from which a value for Young's modulus  $E_b=17$  MPa is obtained. This value is used in FEM simulations for predicting the elastic deformation of bonds. If the bond material deformation exceeds 0.2 strain, then it is out of the linear elastic range. Figure 10 illustrates the tensile engineering stress-strain curve of the rubber-like bond material, with the applied load parallel to the printed layers using ASTM D638 standard (ASTM, 2008) test method. The slope of the tensile stress-strain curve decreases with increased strain, and there is no clear linear range in the curve. The tangent tensile modulus at 0.1 strain is 20 MPa, which will be used as a reference value for comparing FEM predictions with experimental results of doublet deformation. Based on the experimental characterisation results, the material Young's modulus values used in FEM simulations are presented in Table 3. It should be noted that the corresponding Young's modulus for the bonds in DEM is actually different from that connecting the surfaces of the adjacent particles in the experiments, which is addressed below.

<Figure 9. Experimental uniaxial compression engineering stress-strain curves for 3D printing materials (perpendicular loading direction).>

<Figure 10. Experimental tensile engineering stress-strain curves for rubber-like bond material (DM 9895, parallel loading direction).>

<Table 3. Material Young's modulus used in simulations>

### **3.2 Bond characteristics inferred from doublet tests**

To measure the bond stiffness and strength, compression and tensile tests were performed on doublets with different bond size. Detailed test types and results are illustrated in Figures 11-14. FEM analysis was used to determine the linear elastic deformation range of the bonds, where the TBBM model applies, and the results are also shown in the same figures. The bond length,  $l$ , represents the minimum distance between the surfaces of the two particles. For instance, bond length  $l = 0.25$  mm used in experiments corresponds to  $L_b = 4.25$  mm used in DEM simulations.

### 3.2.1 Doublet load-displacement curves

In Figure 11 (a), the experimental compressive force-displacement curves of doublets with different bond lengths are presented. As shown in Figure 11 (a), in experiments, it is possible to obtain the compressive force-displacement curve to 2 mm displacement with a small portion of it is linear. At larger displacements, the three shortest bonds show evidence of yielding behaviour of primary particles (Ge et al., 2018), and the longest bond ( $l=1$  mm) shows a clear failure point at around 1.25 mm displacement. As the particle material is much stiffer than the bond material, at the initial loading stage the deformation mainly takes place at bonds, while for large deformations when two particles in contact both the inter-particle bond and the two particles contribute to the overall deformation. The deformation is analysed by FEM for calibrating the bonding parameters in DEM simulations.

As the 3D printing materials show non-linear characteristics (see Figures 9 and 10), it is necessary to define the linear elastic range of doublet deformation. FEM can capture the effects of the concave ends of the inter-particle bonds (where they are joined to the outer surface of the spherical particles). It offers a way to evaluate the range of linear elastic deformation of inter-particle bonds, based on which the bonding parameters used in the TBBM model can be set. The FEM predictions of doublet deformation during the initial loading stage are plotted in Figure 11 (b). When the bond length  $l=0$  mm, the experimental compressive load differs markedly from FEM prediction. Figure 12 illustrates the FEM simulation results of von Mises stress distributions when two particles are in contact. The large stress is mainly concentrated near the contact point, indicating the place where the initial failure occurs. During compression experiments, it is hardly to observe the state of the bond material at the contact point. It is worthwhile to further investigate the deformation and failure behaviours when two particles are in contact ( $l=0$ ). For the other three cases with relatively longer bonds, the experimental results fit well with FEM predictions, especially at the initial displacements.

<Figure 11. Typical compressive force-displacement curves of doublets with bonds of 2.6 mm diameter and different lengths in perpendicular loading direction: (a) experimental results; (b) FEM simulations for demonstrating elastic deformation at the initial stage shown in the dotted square in (a).>

<Figure 12. Von Mises stress distributions when two particles are in contact under compression loading (Bond length  $l=0$ ). >

Figure 13 presents the tensile force-displacement relationships for different bond lengths for the case in which the printed layers are parallel to the loading direction. The tensile load increases at the beginning and reaches a peak force for each case, which represents the failure of the bond material (Figure 12 (a)). Necking effect can be distinguished near the peak load. After this point, the tensile load decreases rapidly with a further increase of displacement, indicating the inter-particle bond rupture. For all experimental conditions, the tensile stiffness increases with decreasing bond length, and the stiffness values drop as the tensile displacement increases. The experimental results and FEM predictions are compared in Figure 13 (b). In all cases, the experimental tensile results show strong non-linear characteristics, with the experimental loads being far lower than the FEM predicted loads at the same strain. This differs markedly from the compressive loading as shown in Figure 11, as the bond material shows no clear linear elastic range under tensile loads.

Compared with the FEM predictions of doublets, the experimental results of both compression and tensile tests are influenced by the non-linear behaviour of polymers. Nonetheless, for the doublet bond length  $l>0$ , the compressive deformation of doublets at the initial stage show a linear elastic response (see Figure 11 (b)), for which bond Young's modulus can be calculated to be used in the TBBM model. It should be noted that the actual value of Young's modulus of the bond material cannot be used directly in DEM simulations, as the bond length  $l$  is different from that of the simulation, i.e. centre to centre distance  $L_b$ . Therefore some calibration is necessary which is described in section 3.2.3.

<Figure 13. Typical tensile force-displacement curves of doublets with bonds of 2.6 mm diameter and different lengths in parallel loading direction: (a) experimental results; (b) FEM simulations for demonstrating elastic deformation at the initial stage shown in the dotted square in (a).>

### 3.2.2 Calculation of bond stiffness

The bond compressive stiffness,  $k$ , at a given displacement is determined by calculating the



slope of the corresponding load-displacement curves.

$$k = \frac{dF}{du} \quad (8)$$

where  $F$  is compressive loads, and  $u$  is the corresponding displacement. Here, three different bond lengths are considered ( $l=0.25, 0.5, 1$  mm).

The calculated compressive stiffness values are presented in Figure 14. For all the experimental conditions, the compressive stiffness increases with decreasing bond length, and the stiffness values show a slight upward trend as the displacement increases. Due to the 3D printed layer effect, the compressive stiffness is different in different loading directions. Generally, the “perpendicular loading direction” has a higher stiffness with a lower standard deviation than the “parallel loading direction”. In the following, the average compressive stiffness values in the linear elastic range are used to determine the bond Young’s modulus in TBBM.

<Figure 14. Doublet compressive stiffness with  $d=2.6$  mm bond diameter (Results in parallel direction are listed only for reference).>

### 3.2.3 Calibration of the bond Young’s modulus in TBBM

In DEM simulations using the TBBM contact model, the bond characteristic length,  $L_b$ , is defined as the distance between two primary particle centres (Figure 15 (a)), which is longer than the real bond length  $l$  used in the experiments (Figure 15 (b)). This difference influences the resulting deformation in simulation as the bond in this case is more compliant. Therefore, it is necessary to calibrate the bond Young’s modulus using the experimental doublet results which have a real bond length  $l$ , so that the same applied force leads to the same deformation at a given stiffness.

As shown in Figure 15, for the two bonding systems, to obtain the same incremental deformation  $\Delta L$  under the same applied load  $F$ , the following equation needs to be satisfied:

$$\Delta L = \frac{F \cdot L_b}{E_{b,c} \cdot A_b} = \frac{F \cdot l}{E_b \cdot A_b} \quad (9)$$

where  $A_b$  is the bond cross sectional area in TBBM model,  $E_b$  is Young's modulus of bond material. The calibrated bond Young's modulus,  $E_{b,c}$ , in DEM is then obtained as:

$$E_{b,c} = \frac{F \cdot L_b}{\Delta L \cdot A_b} \quad (10)$$

The measured compressive stiffness  $k_c$  of different bond sizes has previously been obtained (see Figure 14). The calibrated bond Young's modulus,  $E_{b,c}$ , for use in DEM is then determined as follows and presented in Table 4:

$$E_{b,c} = \frac{k_c \cdot L_b}{A_b} \quad (11)$$

The results in Table 4 show that the calibrated bond Young's modulus should be reduced with increasing bond length to give the same compliance as the experimental case, but it is obviously larger than the corresponding Young's modulus of the bond material, i.e. 17 MPa. In addition, the calibrated bond Young's modulus is different for the two loading directions relative to the 3D printed layers, with the loading direction perpendicular to the printed layers resulting in significantly higher values. For the agglomerate structures used in this work, the physical bond length  $l$  is 0.25 mm, and the corresponding calibrated bond Young's modulus used in simulations is 136 MPa for perpendicular loading directions (see Table 4), as compared to 17 MPa bond material Young's modulus used in FEM simulations (see Table 3).

<Figure 15. Comparison of bond geometries (a) as defined in the TBBM (b) the geometry as 3D printed in the experiments.>

<Table 4. Calibrated bond Young's modulus  $E_{b,c}$  of different bond lengths (Bond diameter  $d_b=2.6$  mm)>

### 3.3 Experimental results of agglomerate deformation and DEM simulation

The experimental and numerical load-displacement curves are compared in Figures 16 and 17 for the cubic tetrahedral and spherical random structured agglomerates, respectively. As shown in Figure 16, using the calibrated modulus  $E_{b,c}$  for the cubic tetrahedral structured agglomerate, the simulation predictions are in close agreement with the experimental results during the initial deformation (about 4 %) with a displacement less than 1 mm. As for the spherical random structured agglomerate (see Figure 17), when the calibrated bond Young's modulus  $E_{b,c}$  is used, the predicted compressive load fits well with the corresponding experimental result only when the displacement is less than about 0.4 mm. However, a discrepancy appears at larger compressive displacements (>0.4 mm). For interpreting this discrepancy, the bond stress and strain results from DEM and FEM simulations are analysed in the following.

The contact force network and associated bond stress distribution, colour coded in the adjacent bar, are shown in Figure 18. The bond stress values shown in this figure are the quadratic mean of three maximum stress components, i.e. compression ( $\sigma_{Cmax}$ ), tensile ( $\sigma_{Tmax}$ ), shear ( $\tau_{max}$ ). With increased compressive displacement, force chains are formed through the whole structure. For the cubic tetrahedron structure, the bonds inside the structure deform uniformly during compression (see Figure 18 (a)). The structure can sustain linear elastic deformation until much larger deformation. In contrast, the non-uniformly distributed stress field in the case of spherical agglomerate indicates that the bonds at the contact regions can reach the non-linear range at a small compression displacement (see Figure 18 (b)). Figure 19 illustrates the strain range of each individual bond inside the agglomerate structures from DEM simulations. The bond strain  $\varepsilon_b$  is defined as:

$$\varepsilon_b = \frac{|L_b - L_{Dis}|}{L_b} \quad (12)$$

where  $L_b$  is the original center to center distance of two bonded particles, and  $L_{Dis}$  is the center to center distance after deformation. For the cubic tetrahedral structured agglomerate, the maximum bond strain is less than 15 % when the displacement is 1 mm. By contrast, due to non-conformal contact deformation of the spherical random structured agglomerate, the maximum bond strain is around 50 % for the spherical random structured agglomerate under

the same displacement. The high bond strain values inside the spherical random structured agglomerate illustrate that some bond deformations exceed the linear elastic range of experimental bond material, and this is reflected in the results in Figure 17.

The total bond stresses including compressive ( $\sigma_{Cmax}$ ), tensile ( $\sigma_{Tmax}$ ) and shear ( $\tau_{max}$ ) components with respect to the compressive displacement are shown in Figure 20. In this figure, the total bond stress is a sum of the maximum stress of each individual bond in an agglomerate structure. For both structures, the bond stresses increase linearly with increased displacement. During the deformation, the compressive/tensile stress inside the bonds play a dominate role. There are shear stresses emanating from torsional and direct shear deformation of the bonds, accounting for a small portion of the bond stress. In future, it is necessary to experimentally measure the torsional properties of the bond, for making a better comparison between the experiments and simulations. Another point for explaining the different responses between experiments and DEM simulations is the stress distribution inside an inter-particle bond. Figure 21 presents the FEM simulation results of von Mises stress distributions inside a concave-shaped bond. When under compressive loadings, the stress distribution is inhomogeneous, and the maximum stress occurs at the centre of the bond. This bond stress distribution is different with that of a cylindrical beam used in TBBM model. At a large compression displacement, the central region inside the bond exceeds the linear elastic deformation range (Figure 21 c and d).

<Figure 16. Comparison of compression load-displacement curves of experimental and DEM simulation results for the cubic tetrahedral structured agglomerate (Bond diameter  $d=2.6$  mm, bond length  $l=0.25$  mm, and perpendicular loading direction with respect to the printed layers).>

<Figure 17. Comparison of compression load-displacement curves of experimental and DEM simulation results for the spherical random structured agglomerate (Bond diameter  $d=2.6$  mm, average bond length  $l=0.25$  mm, and perpendicular loading direction with respect to the printed layers).>

<Figure 18. Bond stress distributions inside the agglomerate structures as a function of displacement obtained from DEM simulations.>

<Figure 19. The strain range of each individual bond inside the agglomerate structure under different compression placement.>

<Figure 20. Total bond stress inside the agglomerate structures as a function of displacement obtained from DEM simulations.>

<Figure 21. Von Mises stress distributions inside an inter-particle bond under compression loading (Bond length  $l=0.25$  mm).>

Nevertheless, the comparison of results in Figures 16 and 17 reveals that, using the calibrated bond Young's modulus, the DEM simulations can capture the initial deformation of agglomerate structures under compressive loads, based on the characterisation of the individual doublet bond without any fitting parameters.

#### **4. DISCUSSION AND FUTURE WORK**

In this work, we conducted experimental testing of 3D printed particle models at different scales, i.e. single material, doublet and agglomerate scale. By using multi-material 3D printing technology, the agglomerate structure and its sub-models can be precisely controlled and printed. Multiple identical test samples were printed and subjected to standard experimental testing. The obtained experimental results were used for comparing and validating DEM simulations.

The results in this work demonstrate proof-of-concept of how to use 3D printed agglomerates to validate a DEM model of agglomerate deformation. We conducted testing of a 3D printed agglomerate structure, which is a “physical twin” of its digital equivalent within the DEM simulation, and compared the results. By performing doublet tests of bond deformation, the bonding parameters in DEM simulations were carefully measured and calibrated. The comparison of DEM simulations and the experimental results showed that for both structures, i.e. cubic tetrahedral structure and spherical random structure, simulation results can capture the compressive loads during the initial elastic deformation stage provided the compliance of the bond in TBBM model is adjusted to represent the actual bond length. The TBBM model combined with DEM simulation offers a possible way to investigate the elastic deformation of particle assemblies. We have shown that the new method can currently only be applied to the

structures with small elastic deformations for which the linear elastic assumptions of the TBBM model are applicable. The symmetrical agglomerate has a simpler force transmission pattern which allows the elastic region to persist for longer during the initial deformation, but the more accurate modelling of non-symmetric agglomerates with random particle positions is a larger challenge we are trying to address. It is important to note that the TBBM model was chosen for this study based on the physical similarities of the inter-particle bonds we designed and the TBBM model concept of deformation of a stubby beam.

The study has also highlighted several issues that require further consideration. In this work, only compression and tensile test results of the individual doublet bond are reported (Figure 11 and Figure 13); other doublet tests for obtaining the shearing, bending and twisting stiffness of the bonds also need to be conducted in future research. The measured bond stiffness under different loading directions can make a better prediction of the agglomerate deformation. The material behaviour modelled in DEM simulations is commonly assumed to be “ideal” linear elastic. However, 3D printing materials are complex non-linear polymers and the printed layers have anisotropic characteristics that need to be taken into account. As illustrated in Figures 9 and 10, the 3D printing materials show non-linear behaviours at large deformations. Using FEM simulation as a benchmark, we demonstrated that when under compression the bond material between primary particles mainly deforms in a linear elastic way at low displacement (Figure 11). The particle and bond materials may interact and deform simultaneously when the two particles are in contact ( $l=0$ ). The non-linear deformation of contacts is influenced by the concave geometry of bonds, elastic-plastic deformation of particles and non-linear elastic behaviour of the bond materials. Apart from this, the bond stiffness is different under different loading directions with respect to the 3D printed layers (see Figure 14). In this work, agglomerates were tested under controlled directions, i.e. 3D printed layers were kept perpendicular to the loading direction. Although this anisotropy is notable in 3D printed agglomerates, many industrial materials also exhibit anisotropic deformation and strength. Crystalline materials can have slip and cleavage planes and weaknesses in certain orientations and any agglomerate bridge containing small needle-shaped crystals, as has been observed in pharmaceutical bridges (Farber et al., 2003), is also highly likely to show differences in bridge strength depending on the direction of the load. We anticipate that in future rapidly developed 3D printing technology can overcome these issues, and new particle models being developed may also capture such complexities (Shen et al., 2016).

In summary, this study rigorously validated DEM modelling of agglomerates at small extents of strains and highlighted a range of behaviours – non-linear material behaviours, anisotropic bond strengths – that posed a challenge to the predictive capabilities of DEM modelling of agglomerates, thus requiring further developments. The multi-material 3D printed agglomerates offer a unique opportunity to study this non-standard deformation and breakage behaviour using a highly controllable and reproducible multiscale experimental approach. This opens up the chance for significant advances in agglomerate deformation and breakage modelling in future.

## **5. CONCLUSIONS**

In this research, we proposed a novel multiscale experimental approach for comparing and validating particle models. Multi-material 3D printing was applied to produce agglomerate structures and their sub-models. Mechanical tests were performed on these 3D printed samples from single material to agglomerate scale. For the numerical simulation, a DEM simulation of an agglomerate with matching structure and bond properties was conducted using the newly developed TBBM contact model.

The main contributions and findings of this work are as follows:

1. For the first time, using multi-material 3D printing technology, we produced agglomerate structures with well controlled and characterised material properties, which enabled a precise comparison of experiment and numerical simulations of agglomerate deformation.
2. Using doublet tests, the inter-particle bond stiffness and strength of different dimensions were carefully measured and analysed. FEM simulation was used to define the linear elastic deformation limit of bonds. This enabled the physical properties and bonding parameters for the DEM simulations to be measured exactly for the first time.
3. Quasi-static uniaxial compression tests were performed experimentally and compared to DEM simulations of the agglomerate deformation behaviour. A calibrated Young's modulus for the doublet bond was used to predict the elastic deformation of agglomerate structures. For both structures used in this work, i.e. cubic tetrahedral structure and spherical random structure, DEM simulation combined with TBBM model can capture the extent of deformation as a

function of the compressive load at the initial elastic stage. The discrepancy between experiments and DEM simulations at large compressive displacements is interpreted by DEM and FEM simulation results.

This paper successfully demonstrated the concept of using a coordinated multiscale approach to match the physical and digital agglomerate structures and properties. By using 3D printing technology, the agglomerates discussed here have the most reproducible physical properties ever made. This offers new opportunities to advance computational particle technology.

## LIST OF SYMBOLS

$A$	Area ( $\text{m}^2$ )
$d$	Diameter (m)
$E$	Young's modulus (Pa)
$F$	Force (N)
$I$	Second moment of area ( $\text{m}^4$ )
$K$	Stiffness ( $\text{N m}^{-1}$ )
$k$	Stiffness constant ( $\text{N m}^{-1}$ )
$L$	Bond length used in TBBM model (m)
$l$	Bond length that represents the minimum distance between the particles (m)
$M$	Moment (N.m)
$r$	Radius (m)
$u$	Displacement vector (m)
$\varepsilon$	Strain (-)
$\sigma$	Compressive/Tensile strength (MPa)
$\tau$	Shear strength (MPa)

### Indices

$\alpha, \beta$	Ends of a single beam
$b$	Bond
$C$	Compressive stress
$c$	Compressive stiffness
$Dis$	Deformation displacement
min	Minimum



max	Maximum
$p$	Particle
$T$	Tensile stress
$x, y, z$	Cartesian coordinates

## ACKNOWLEDGEMENTS

This research project was supported by International Fine Particle Research Institute (IFPRI) and an ARC Discovery grant (DP150100119). Ruihuan Ge's PhD scholarship was supported by the China Scholarship Council (CSC). The authors would also like to acknowledge Dr Wenguang Nan at the University of Leeds for discussing the DEM simulations. The support of DEM Solutions for providing EDEM licences for the purpose of this work is greatly acknowledged.

## REFERENCES

- PolyJet Materials, p. available online at <http://www.stratasys.com/materials/polyjet>.
- Instron Corporation, 2005. Instron Series 5500 Load Frames Reference Manual.
- ASTM, D., 2008. 638-03: Standard Test Method for Tensile Properties of Plastics. Current edition approved Apr 1, 1-16.
- Brown, N.J., 2013. Discrete element modelling of cementitious materials, PhD dissertation, University of Edinburgh.
- Brown, N.J., Chen, J.-F., Ooi, J.Y., 2014. A bond model for DEM simulation of cementitious materials and deformable structures. *Granular Matter* 16, 299-311.
- Cundall, P.A., Strack, O.D., 1979. A discrete numerical model for granular assemblies. *Géotechnique* 29, 47-65.
- Dadkhah, M., Tsotsas, E., 2014. Study of the morphology of solidified binder in spray fluidized bed agglomerates by X-ray tomography. *Powder technology* 264, 256-264.
- Dale, S., Wassgren, C., Litster, J., 2014. Measuring granule phase volume distributions using X-ray microtomography. *Powder Technology* 264, 550-560.
- Derjaguin, B.V., Muller, V.M., Toporov, Y.P., 1975. Effect of contact deformations on the adhesion of particles. *J Colloid Interface Sci* 53, 314-326.

- Dosta, M., Dale, S., Antonyuk, S., Wassgren, C., Heinrich, S., Litster, J.D., 2016. Numerical and experimental analysis of influence of granule microstructure on its compression breakage. *Powder Technology* 299, 87-97.
- Eckhard, S., Fries, M., Antonyuk, S., Heinrich, S., 2017. Dependencies between internal structure and mechanical properties of spray dried granules—Experimental study and DEM simulation. *Advanced Powder Technology* 28, 185-196.
- Ergenzinger, C., Seifried, R., Eberhard, P., 2011. A discrete element model to describe failure of strong rock in uniaxial compression. *Granular Matter* 13, 341-364.
- Farber, L., Tardos, G.I., Michaels, J.N., 2003. Evolution and structure of drying material bridges of pharmaceutical excipients: studies on a microscope slide. *Chemical Engineering Science* 58, 4515-4525.
- Ge, R., Ghadiri, M., Bonakdar, T., Hapgood, K., 2017. 3D printed agglomerates for granule breakage tests. *Powder technology* 306, 103-112.
- Ge, R., Ghadiri, M., Bonakdar, T., Zhou, Z., Larson, I., Hapgood, K., 2018. Experimental study of the deformation and breakage of 3D printed agglomerates: Effects of packing density and inter-particle bond strength. *Powder technology* 340, 299-310.
- Ge, R., Wang, L., Zhou, Z., 2019. DEM analysis of compression breakage of 3D printed agglomerates with different structures. *Powder technology* 356, 1045-1058.
- Golchert, D., Moreno, R., Ghadiri, M., Litster, J., Williams, R., 2004. Application of X-ray microtomography to numerical simulations of agglomerate breakage by distinct element method. *Advanced Powder Technology* 15, 447-457.
- Johnson, K., Kendall, K., Roberts, A., 1971. Surface energy and the contact of elastic solids, *Proceedings of the Royal Society of London A: Mathematical, Physical and Engineering Sciences*. The Royal Society, pp. 301-313.
- Kafui, K., Thornton, C., 1993. Computer simulated impact of agglomerates. *Powders and Grains* 93, 401-406.
- Liu, L., Kafui, K.D., Thornton, C., 2010. Impact breakage of spherical, cuboidal and cylindrical agglomerates. *Powder Technology* 199, 189-196.
- Matuttis, H.-G., Schinner, A., 2001. Particle simulation of cohesive granular materials. *International Journal of Modern Physics C* 12, 1011-1021.
- Mishra, B., Thornton, C., 2001. Impact breakage of particle agglomerates. *International Journal of Mineral Processing* 61, 225-239.

- Moreno-Atanasio, R., Ghadiri, M., 2006. Mechanistic analysis and computer simulation of impact breakage of agglomerates: Effect of surface energy. *Chemical Engineering Science* 61, 2476-2481.
- Potyondy, D.O., Cundall, P.A., 2004. A bonded-particle model for rock. *International Journal of Rock Mechanics and Mining Sciences* 41, 1329-1364.
- Przemieniecki, J.S., 1985. *Theory of matrix structural analysis*. Courier Corporation.
- Reynolds, G.K., Fu, J.S., Cheong, Y.S., Hounslow, M.J., Salman, A.D., 2005. Breakage in granulation: A review. *Chemical Engineering Science* 60, 3969-3992.
- Shen, Z., Jiang, M., Thornton, C., 2016. DEM simulation of bonded granular material. Part I: Contact model and application to cemented sand. *Computers and Geotechnics* 75, 192-209.
- Subero, J., Ning, Z., Ghadiri, M., Thornton, C., 1999. Effect of interface energy on the impact strength of agglomerates. *Powder Technology* 105, 66-73.
- Subero, J., Pascual, D., Ghadiri, M., 2000. Production of Agglomerates of Well-Defined Structures and Bond Properties Using a Novel Technique. *Chemical Engineering Research and Design* 78, 55-60.
- Takezawa, A., Kobashi, M., Kitamura, M., 2015. Porous composite with negative thermal expansion obtained by photopolymer additive manufacturing. *APL Materials* 3, 076103.
- Thornton, C., Ciomocos, M.T., Adams, M.J., 2004. Numerical simulations of diametrical compression tests on agglomerates. *Powder Technology* 140, 258-267.
- Thornton, C., Liu, L., 2004. How do agglomerates break? *Powder Technology* 143-144, 110-116.
- Thornton, C., Yin, K., Adams, M., 1996. Numerical simulation of the impact fracture and fragmentation of agglomerates. *Journal of Physics D: Applied Physics* 29, 424.
- Wang, L., Lau, J., Thomas, E.L., Boyce, M.C., 2011. Co-continuous composite materials for stiffness, strength, and energy dissipation. *Adv Mater* 23, 1524-1529.

## Figures:

Figure 1. Agglomerate design used in this study.

Figure 2. Overview of the design and production process for spherical agglomerates with random internal structure.

Figure 3. 3D printed test samples at three different scales.

Figure 4. Schematic of loading direction with respect 3D printed layers.

Figure 5. Schematic of breakage test setup, showing the horizontal alignment of the print layers with the testing platens.

Figure 6. Schematic of a single beam connecting particles together.

Figure 7. Comparison of simulated load-displacement curves as a function of loading rate for cubic shaped, tetrahedral structured agglomerate.

Figure 8. An axisymmetric FEM mesh setup used in doublet compression simulations.

Figure 9. Experimental uniaxial compression engineering stress-strain curves for 3D printing materials.

Figure 10. Experimental tensile engineering stress-strain curves for rubber-like bond material (DM 9895).

Figure 11. Typical compressive force-displacement curves of doublets (Perpendicular loading direction).

Figure 12. Von Mises stress distributions when two particles are in contact under compression (Bond length  $l=0$ ).

Figure 13. Typical tensile force-displacement curves of doublets (Parallel loading direction).

Figure 14. Doublet compressive stiffness with  $d=2.6$  mm bond diameter (Results in parallel direction are listed only for reference).

Figure 15. Comparison of bond geometries.

Figure 16. Comparison of compression load-displacement curves of experimental and DEM simulation results for the cubic tetrahedral structured agglomerate.

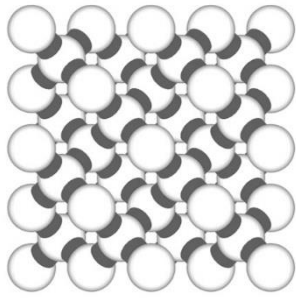
Figure 17. Comparison of compression load-displacement curves of experimental and DEM simulation results for the spherical random structured agglomerate.

Figure 18. Bond stress distributions inside the agglomerate structures as a function of displacement obtained from DEM simulations.

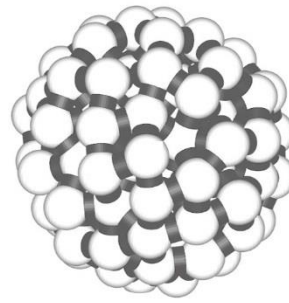
Figure 19. Total bond stress inside the agglomerate structures as a function of displacement obtained from DEM simulations.

Figure 20. The strain range of each individual bond inside the agglomerate structure under different compression displacement.

Figure 21. Von Mises stress distributions inside an inter-particle bond under compression loading (Bond length  $l=0.25$  mm).



(a)



(b)

Figure 1. Agglomerate design used in this study: (a) cubic agglomerate with tetrahedral internal structure, and (b) spherical agglomerate with random internal structure.

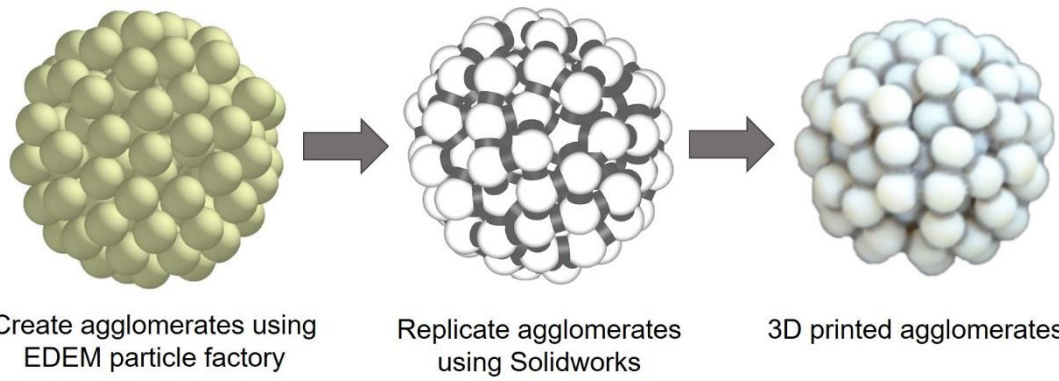


Figure 2. Overview of the design and production process for spherical agglomerates with random internal structure.

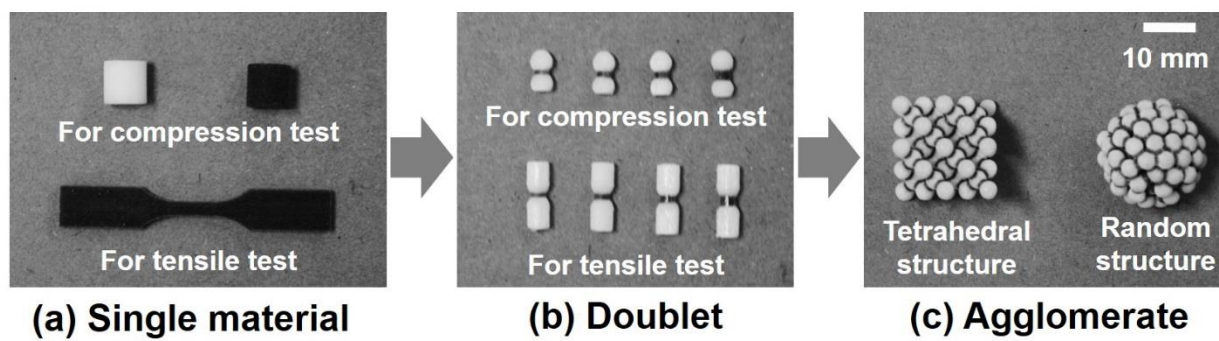
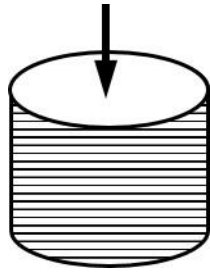
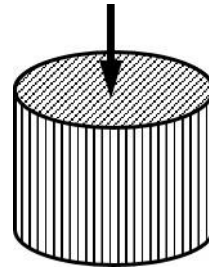


Figure 3. 3D printed test samples at three different scales. White material is a rigid polymer (VeroWhitePlus<sup>TM</sup>), and black material is a rubber-like polymer (DM 9895).





(a) Loading direction perpendicular to printed layer planes



(b) Loading direction parallel to printed layer planes

Figure 4. Schematic of loading direction with respect to 3D printed layers inside a cylindrical geometry.

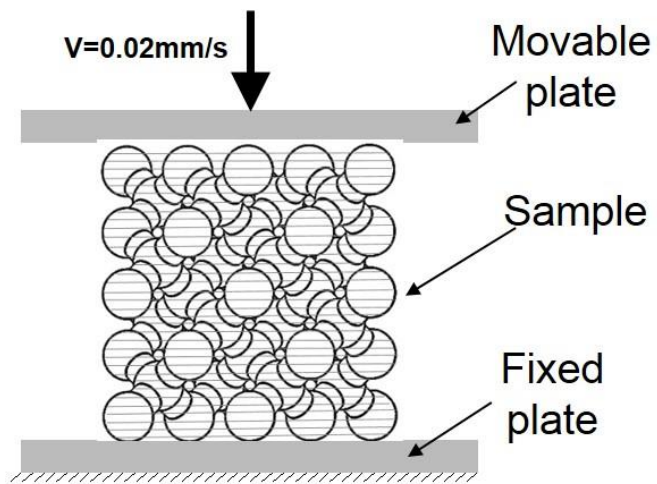


Figure 5. Schematic of breakage test setup, showing the horizontal alignment of the print layers with the testing platens.

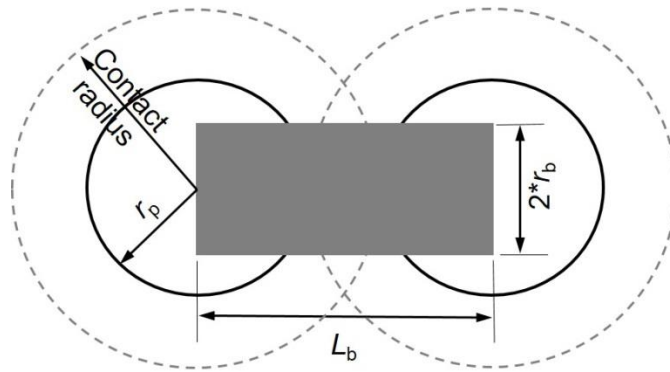


Figure 6. Schematic of a single beam connecting particles together. Particles are bonded together when the contact radius overlaps. The solid circle shows the actual particles, while the broken circle radius and overlap are used to define the bond length. (Particle diameter  $2*r_p= 4$  mm, bond radius  $r_b=1.3$  mm, contact radius is 2.15 mm and 2.28 mm for cubic tetrahedral structure and spherical random structure, respectively)

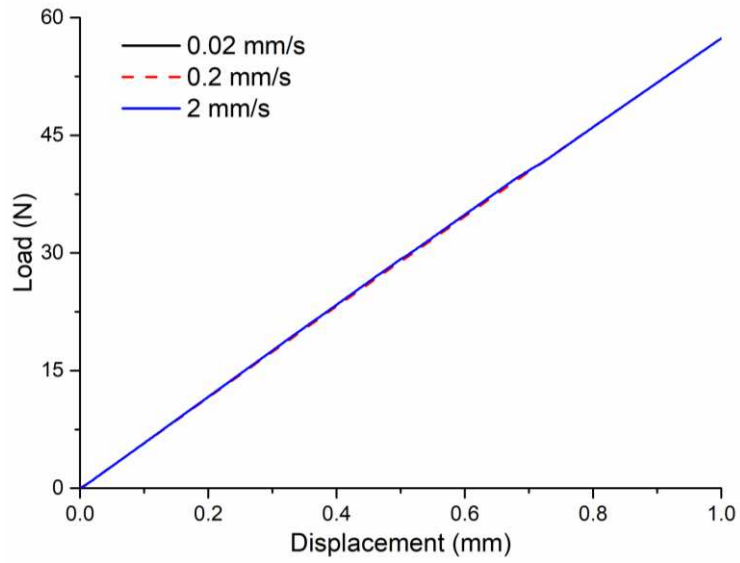
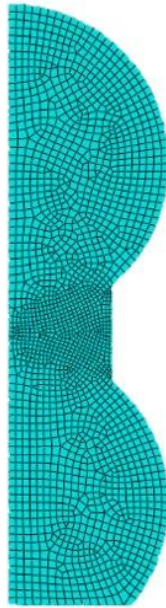
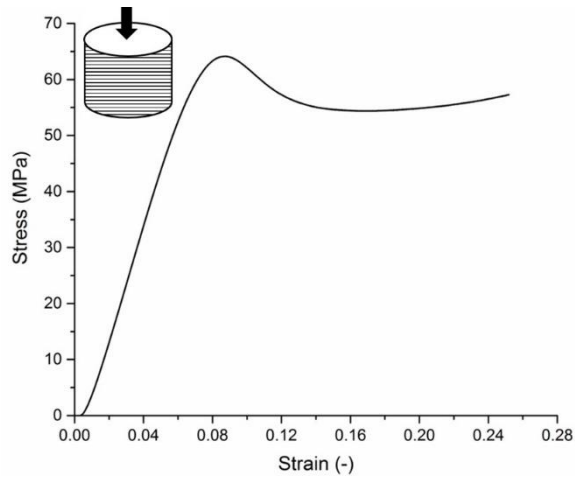


Figure 7. Comparison of simulated load-displacement curves as a function of loading rate for cubic shaped, tetrahedral structured agglomerate.

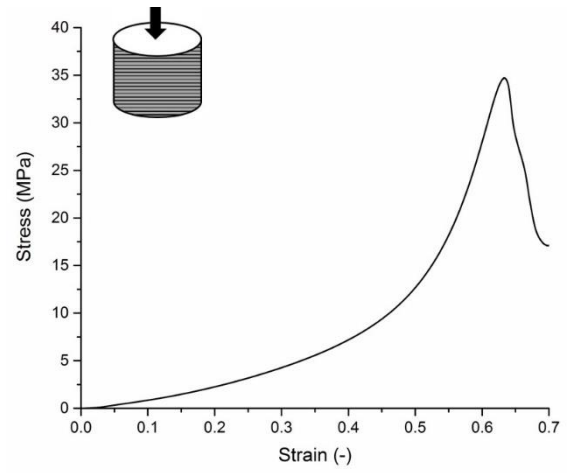


**Particle radius: 2 mm**  
**Bond radius: 1.3 mm**

Figure 8. An axisymmetric FEM mesh setup used in doublet compression simulations.



(a) Rigid material used to make particles (Vero WhitePlus™)



(b) Rubber-like material used to make the bonds (DM 9895)

Figure 9. Experimental uniaxial compression engineering stress-strain curves for 3D printing materials (perpendicular loading direction).

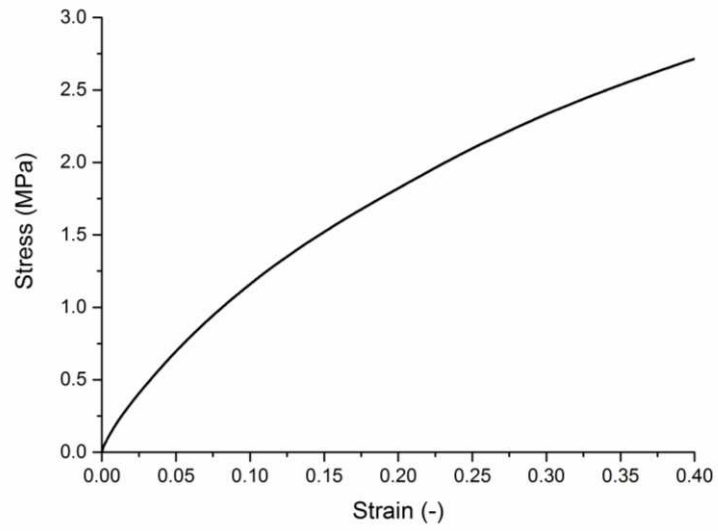
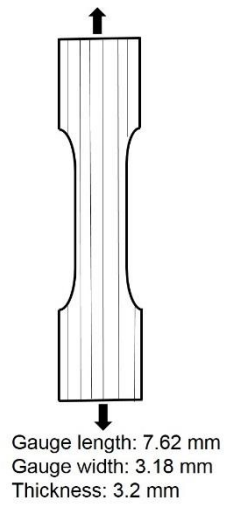
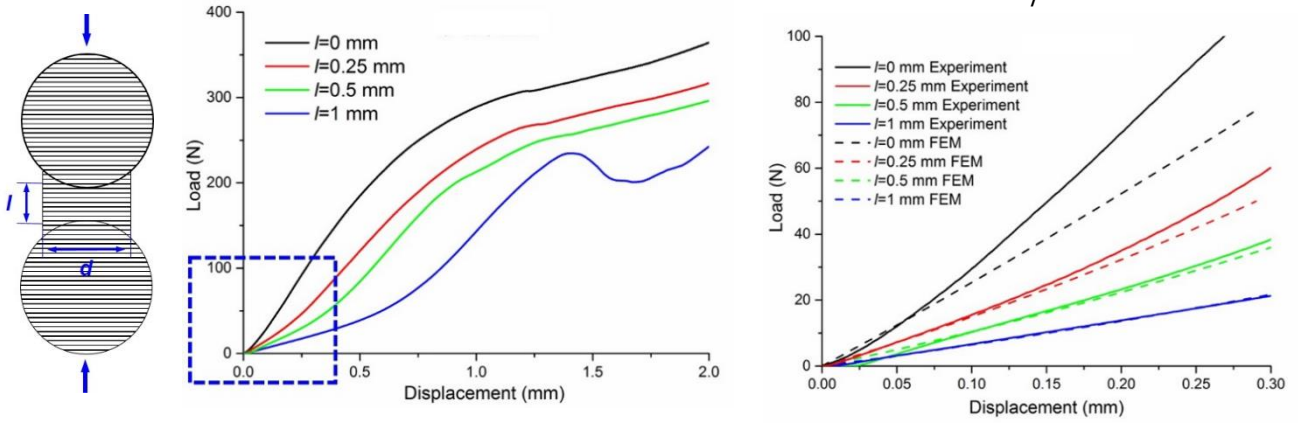


Figure 10. Experimental tensile engineering stress-strain curves for rubber-like bond material (DM 9895, parallel loading direction).



(a) Experimental results

(b) FEM vs Experiment

Figure 11. Typical compressive force-displacement curves of doublets with bonds of 2.6 mm diameter and different lengths in perpendicular loading direction: (a) experimental results; (b) FEM simulations for demonstrating elastic deformation at the initial stage shown in the dotted square in (a).



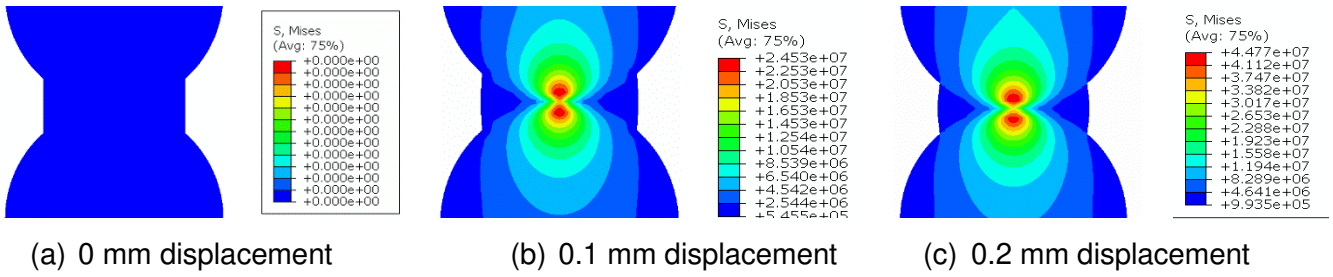
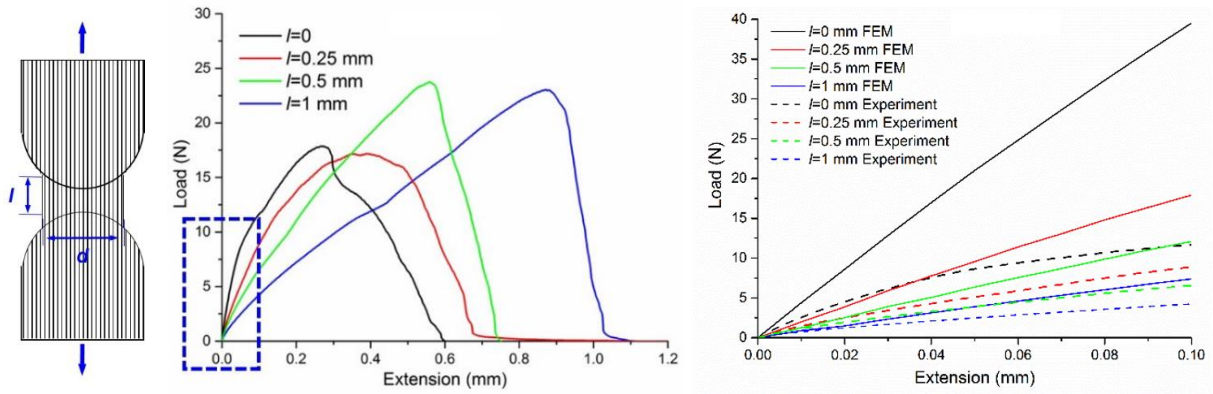


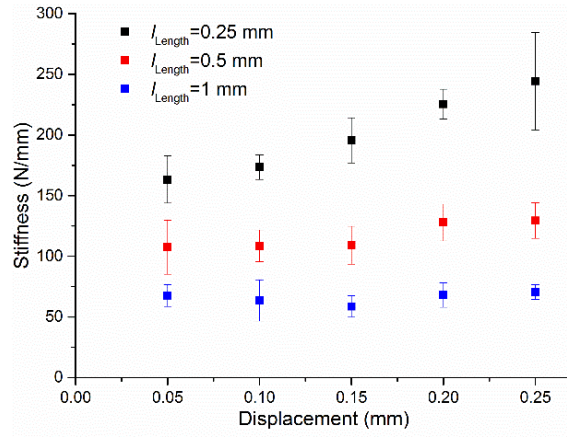
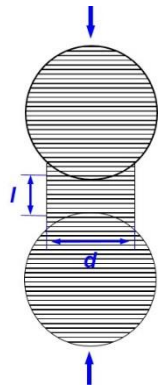
Figure 12. Von Mises stress distributions when two particles are in contact under compression (Bond length  $l=0$ ).



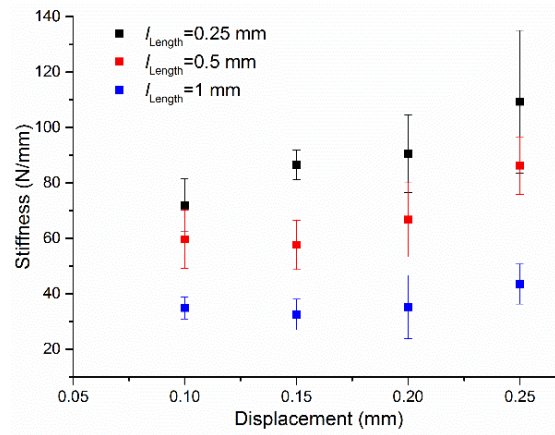
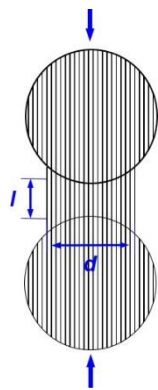
(a) Experimental results

(b) FEM vs Experiment

Figure 13. Typical tensile force-displacement curves of doublets with bonds of 2.6 mm diameter and different lengths in parallel loading direction: (a) experimental results; (b) FEM simulations for demonstrating elastic deformation at the initial stage shown in the dotted square in (a).



(a) Perpendicular loading direction with regards to the printed layers



(b) Parallel loading direction with regards to the printed layers

Figure 14. Doublet compressive stiffness with  $d=2.6$  mm bond diameter (Results in parallel direction are listed only for reference).

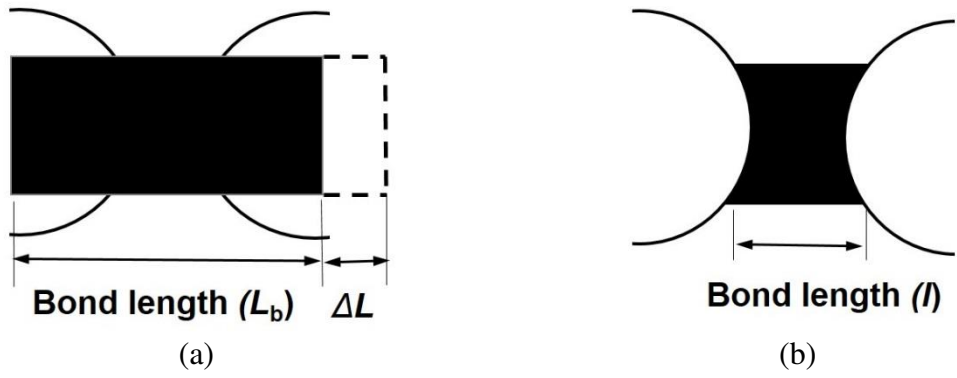


Figure 15. Comparison of bond geometries (a) as defined in the TBBM (b) the geometry as 3D printed in the experiments.

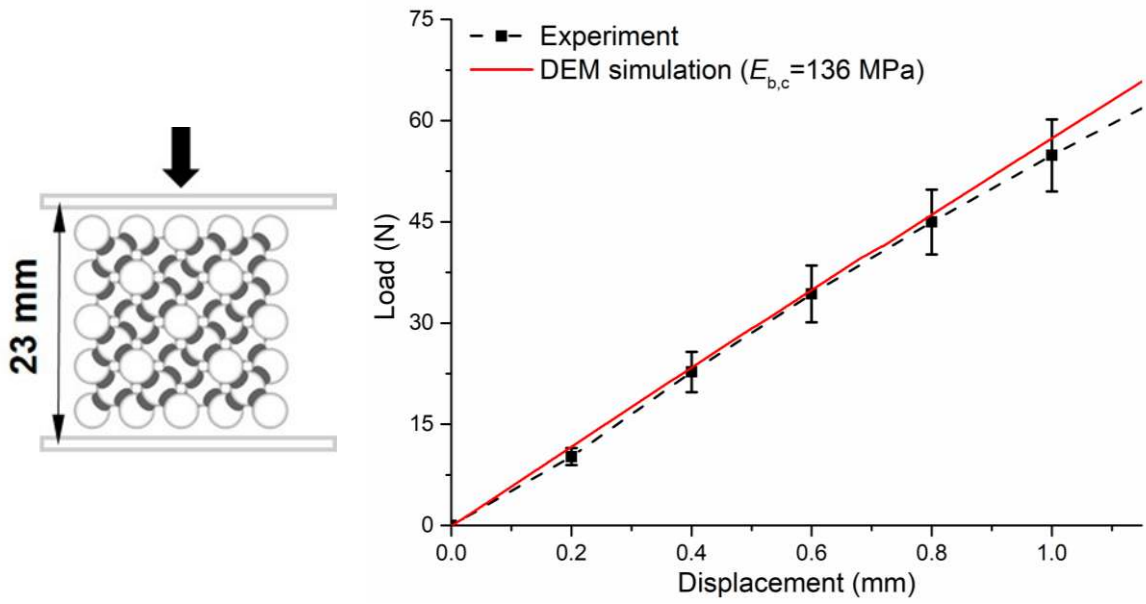


Figure 16. Comparison of compression load-displacement curves of experimental and DEM simulation results for the cubic tetrahedral structured agglomerate (Bond diameter  $d=2.6$  mm, bond length  $l=0.25$  mm, and perpendicular loading direction with respect to the printed layers).

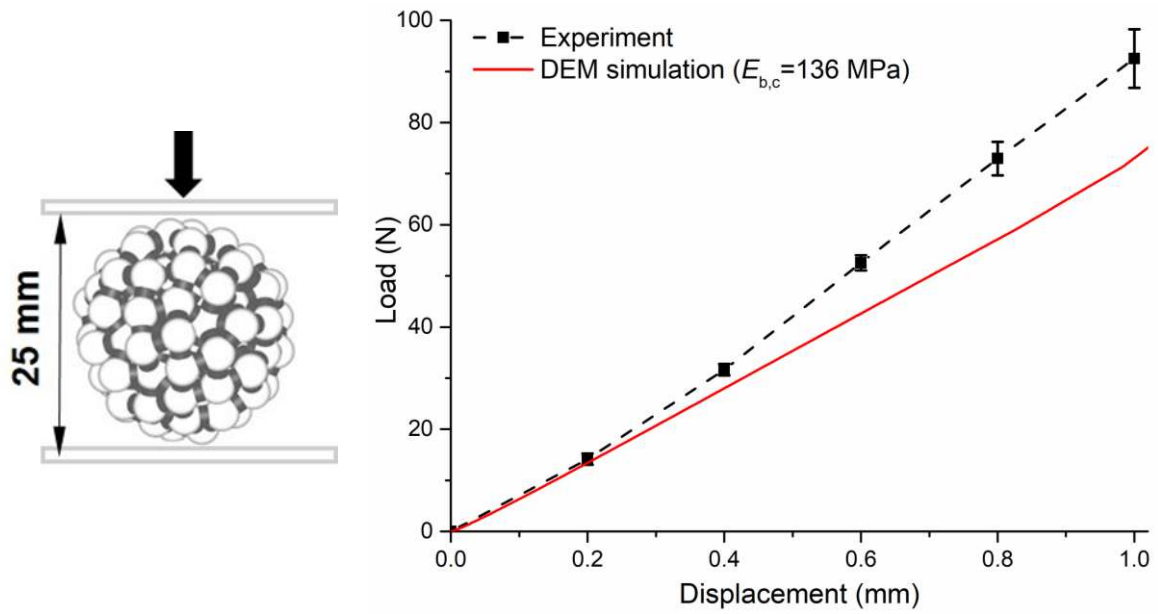
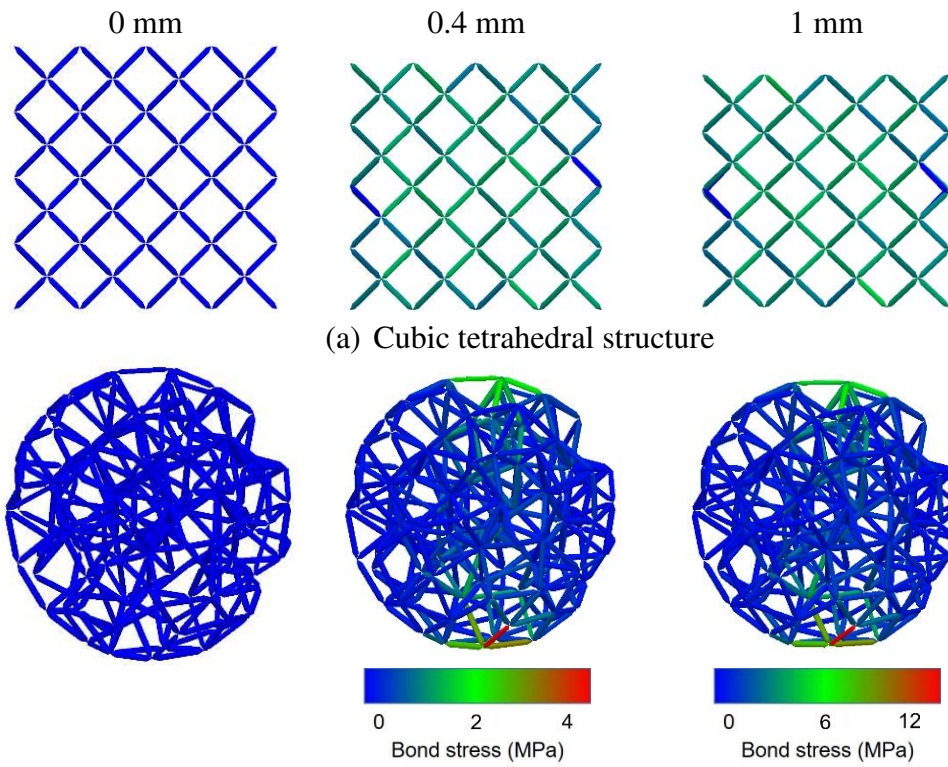


Figure 17. Comparison of compression load-displacement curves of experimental and DEM simulation results for the spherical random structured agglomerate (Bond diameter  $d=2.6$  mm, average bond length  $l=0.25$  mm, and perpendicular loading direction with respect to the printed layers).



(b) Spherical random structure

Figure 18. Bond stress distributions inside the agglomerate structures as a function of displacement obtained from DEM simulations.

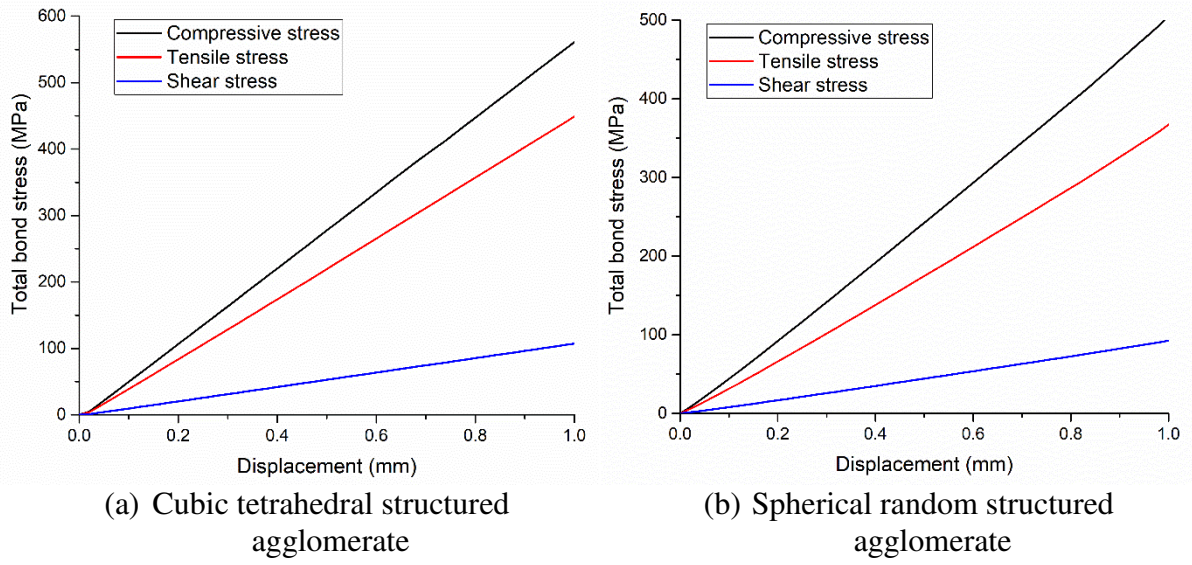
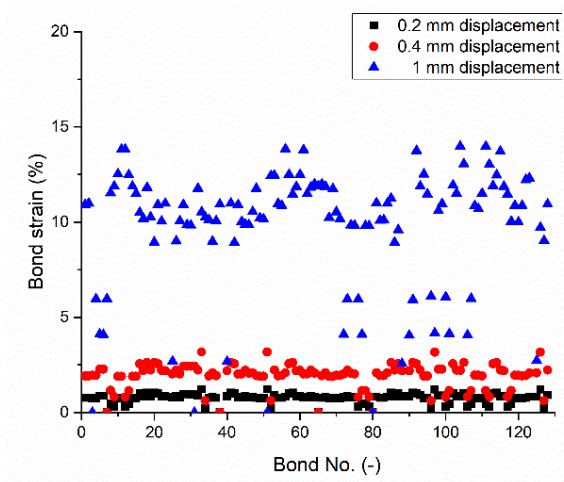
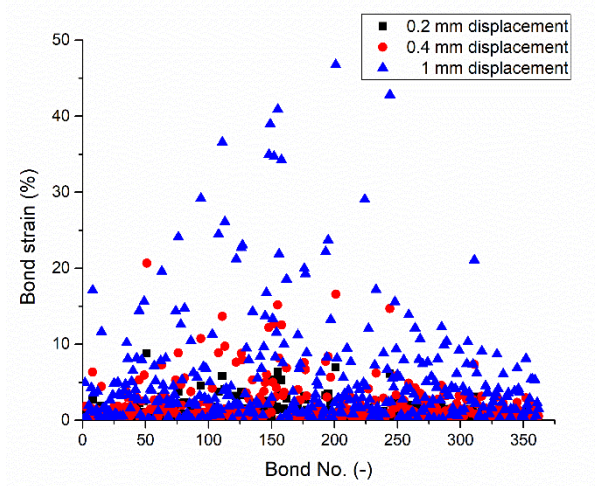


Figure 19. Total bond stress inside the agglomerate structures as a function of displacement obtained from DEM simulations.





(a) Cubic tetrahedral structured agglomerate



(b) Spherical random structured agglomerate

Figure 20. The strain range of each individual bond inside the agglomerate structure under different compression displacement.

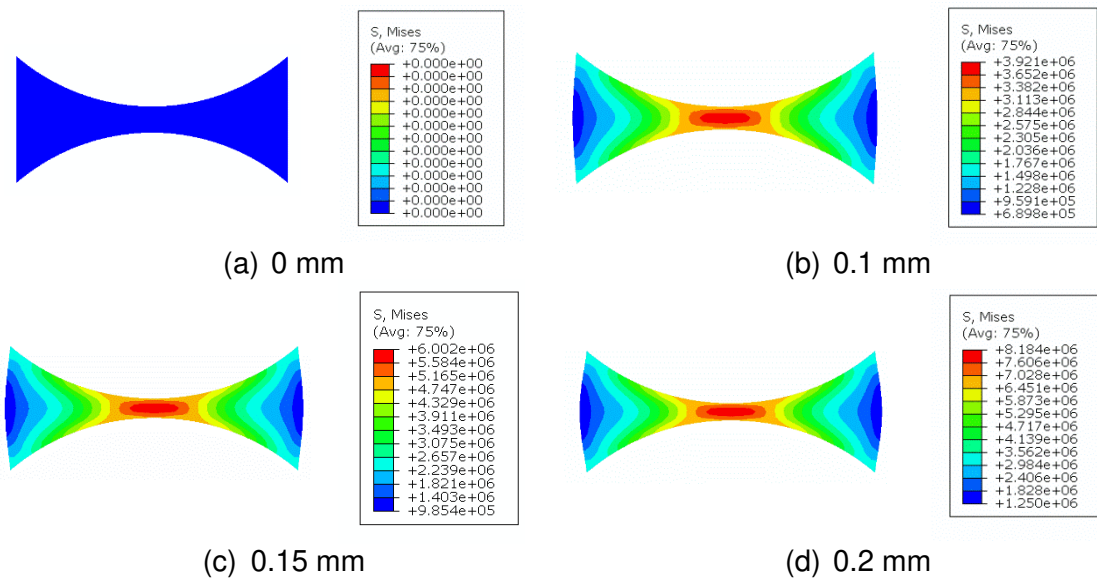


Figure 21. Von Mises stress distributions inside an inter-particle bond under compression loading (Bond length  $l=0.25$  mm).

**Tables:**

Table 1. Measurement dimensions of 3D printed cylinders

Table 2. Parameters used in DEM simulation

Table 3. Material Young's modulus used in simulations

Table 4. Calibrated bond Young's modulus  $E_{b,c}$  of different bond lengths (Bond diameter  $d_b=2.6$  mm)

Table 1. Measurement dimensions of 3D printed cylinders

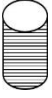
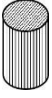

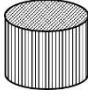
	10 mm height & 4 mm diameter		10 mm height & 10 mm diameter	
	Horizontal alignment	Vertical alignment	Horizontal alignment	Vertical Alignment
				
Height (mm)	$10 \pm 0.07$	$10.1 \pm 0.1$	$10 \pm 0.01$	$10.1 \pm 0.01$
Diameter (mm)	$4 \pm 0.04$	$3.9 \pm 0.06$	$10 \pm 0.04$	$10 \pm 0.04$

Table 2. Parameters used in DEM simulation

<b>Parameter</b>	<b>Description</b>	<b>Value</b>
<b>Bond</b>	Young's modulus (MPa)	136
	Poisson's ratio (-)	0.4
	Compressive strength (MPa)	50
	Tensile strength (MPa)	10
	Shear strength (MPa)	10
	Coefficient of variation of strength (-)	0
	Bond radius multiplier (-)	0.65
<b>Steel platen</b>	Static friction coefficient (-)	0.3
	Coefficient of restitution (-)	0.9
	Density (kg/m <sup>3</sup> )	7800
	Poisson's ratio (-)	0.3
	Shear modulus (GPa)	70
<b>Particle</b>	Diameter (m)	0.004
	Static friction coefficient (-)	0.3
	Coefficient of restitution (-)	0.9
	Density (kg/m <sup>3</sup> )	1200
	Poisson's ratio (-)	0.3
	Young's modulus (MPa)	1100

Table 3. Material Young's modulus used in simulations

<b>Material</b>	<b>Compression test (MPa)</b>		<b>Tensile test (MPa)</b>
	Perpendicular direction	Parallel direction *	
Particle material (Vero White)	1100	900	-
Bond material (DM 9895)	17	9	20

\* Results in parallel direction are listed only for reference.

Table 4. Calibrated bond Young's modulus  $E_{b,c}$  of different bond lengths (bond diameter  $d_b=2.6$  mm) \*

<b>Bond length (<math>l</math>, mm)</b>	<b>Calibrated modulus (<math>E_{b,c}</math>, MPa)</b>	
	Perpendicular direction	Parallel direction
0.25	$136 \pm 16$	$72 \pm 9$
0.5	$91 \pm 18$	$60 \pm 10$
1	$54 \pm 7$	$35 \pm 4$

\* Results in parallel direction are listed for reference. The corresponding Young's modulus of bond material is 17 MPa in perpendicular loading direction and 9 MPa in parallel loading direction.